2005

Increased carrier lifetimes in GaN epitaxial films grown using SiN and TiN porous network layers

Ü. Özgür
Virginia Commonwealth University, uozgur@vcu.edu

Y. Fu
Virginia Commonwealth University

Y. T. Moon
Virginia Commonwealth University

See next page for additional authors

Ozgur, U., Fu, Y., Moon, Y. T., et al. Increased carrier lifetimes in GaN epitaxial films grown using SiN and TiN porous network layers. Journal of Applied Physics 97, 103704 (2005). Copyright © 2005 AIP Publishing LLC.

Increased carrier lifetimes in GaN epitaxial films grown using SiN and TiN porous network layers

Ü. Özgür,[a] Y. Fu, Y. T. Moon, F. Yun, and H. Morkoç
Department of Electrical Engineering, Virginia Commonwealth University, Richmond, Virginia 23284

H. O. Everitt[b]
Department of Physics, Duke University, Durham, North Carolina 27708

(Received 8 December 2004; accepted 24 February 2005; published online 29 April 2005)

Improved structural quality and radiative efficiency were observed in GaN thin films grown by metalorganic chemical vapor deposition on SiN and TiN porous network templates. The room-temperature decay times obtained from biexponential fits to time-resolved photoluminescence data are increased with the inclusion of SiN and TiN layers. The carrier lifetime of 1.86 ns measured for a TiN network sample is slightly longer than that for a 200 μm-thick high-quality freestanding GaN. The linewidth of the asymmetric x-ray diffraction (XRD) $(10\bar{1}2)$ peak decreases considerably with the use of SiN and TiN layers, indicating the reduction in threading dislocation density. However, no direct correlation is yet found between the decay times and the XRD linewidths, suggesting that point defect and impurity-related nonradiative centers are the main parameters affecting the lifetime. © *2005 American Institute of Physics*. [DOI: 10.1063/1.1894583]

I. INTRODUCTION

Technological advances in group-III nitride-based optoelectronic and electrical devices have been made possible owing to extensive materials research, resulting in the commercialization of short-wavelength emitters and detectors.[1] Meanwhile, the motivation for improved devices as well as bringing high-performance electronic devices to the market place is continually driving the GaN technology for improved material quality with better optical and electrical performance. In attaining the current state of nitride device development, overcoming material growth difficulties has been the main focus. Conventional heteroepitaxial growth of GaN on low-temperature GaN or AlN buffer layers deposited on sapphire (Al_2O_3) and SiC substrates results in films containing high density of threading dislocations (TDs) (10^9–10^{10} cm^{-2}) and associated point defects due to lattice mismatch between the film and the substrate. These imperfections affect both the optical and electrical properties, hindering advances in device performance since they scatter charge carriers and reduce the efficiency of radiative recombination.[2]

The best quality GaN epilayers are obtained by using homoepitaxial growth over freestanding GaN templates or bulk GaN; however, at present, the size and growth rate of high-quality bulk crystals are limited. Thick hydride vapor-phase epitaxy (HVPE)-grown GaN templates exhibit very low TD densities (5×10^6 cm^{-2}).[3,4] Currently, to reduce TDs and to obtain device-quality GaN epilayers, the best way is to use the epitaxial lateral overgrowth[5] (ELO) technique; however, the conventional ELO process requires *ex situ* photolithographic preparation that is cumbersome and increases the cost. To overcome this drawback, several groups have reported on the micro-ELO method using an *in situ* grown discontinuous SiN layer as mask.[6–9] The SiN layer is typically deposited on the GaN buffer layer by simultaneously introducing silane and ammonia gases into the metalorganic chemical vapor deposition (MOCVD) reactor. The *in situ* ELO method can significantly reduce the density of threading dislocations and the production cost because all the processes can continuously be performed within the growth chamber.

Another technique to reduce the TD density is to use a TiN interlayer.[12] A thin Ti metal layer is deposited on a thin GaN template by an *e*-beam evaporator and then annealed under an ammonia plus hydrogen atmosphere at >1000 °C in the MOCVD chamber. The thermal annealing process transforms the Ti metal layer to a TiN porous network. Simultaneously, the underlying thin GaN template is thermally etched to form crystalline GaN grains which act as seeds in the subsequent GaN overgrowth process. Although it requires the *ex situ* process of Ti metal layer deposition by an *e*-beam evaporator, the TiN network method is more effective in reducing the dislocation density than the SiN network method due to this initial lateral growth of the GaN seeds.

The application of a TiN interlayer has recently been reported for self-separation of HVPE-grown GaN template (a few hundred microns) from sapphire.[10] A very low TD density of 5×10^6 cm^{-2} was achieved for the GaN grown on the TiN interlayer. However, in these experiments the HVPE GaN layers were very thick (300 μm), and a dislocation density of 10^6 cm^{-2} is already possible in GaN layers grown by the same method without any TiN network.[11] Therefore, the effectiveness of the TiN network method to reduce TD density was unclear.

Here we report the optical characterization of thin GaN epitaxial layers grown by MOCVD on SiN and TiN porous networks. The photogenerated carrier decay times measured

[a]Electronic mail: uozgur@vcu.edu
[b]Also with the U.S. Army Research Office, Research Triangle Park, Durham, NC 27709.

by time-resolved photoluminescence (TRPL) are lengthened as a result of either the SiN or the TiN network. In fact, the lifetimes measured for samples with the TiN interlayer are longer than even that for thick HVPE-grown templates and thin films without the TiN network, indicating the superior quality of the overgrown GaN layers.

II. EXPERIMENTAL DETAILS

Three sets of GaN samples with SiN network were grown with three different 100 nm-thick buffer layers on 6H-SiC substrates which were H etched at 1700 °C to eliminate polishing damage: (1) a low-temperature (LT) (550 °C)-grown GaN buffer, (2) a high-temperature (HT) (950 °C)-grown GaN buffer, and (3) a high-temperature (1090 °C)-grown AlN buffer. A thin porous SiN layer was deposited directly on the buffer layers by interrupting the Ga source flow and flowing diluted silane gas in the presence of ammonia. Partial coverage of the buffer layer achieved by short deposition times formed the porous SiN structure. This was followed by GaN overgrowth at 1000, 1030, and 1050 °C for the LT-GaN, HT-GaN, and AlN buffer layer samples, respectively. The growth pressure was 30 Torr, and the NH_3 to Ga source flow ratio (V/III ratio) was kept at 2000. For each of the three sets, one control sample with no SiN nanonetwork, one sample with a single SiN network layer, and a third sample with double SiN network layers were grown. For the double SiN layer growth, a second SiN layer was deposited after the deposition of 2 μm of GaN on the first SiN layer. The total thickness of each sample was 5 μm. There was no intentional doping in any of the samples.

For the TiN network template preparation, 10-nm Ti films were *e*-beam evaporated on 0.7 μm-thick MOCVD-grown GaN templates, then subjected to *in situ* thermal annealing at 1050 °C in a fixed ratio of NH_3 to H_2 (1:3) gases inside the MOCVD chamber at 200 Torr. Critical parameters for TiN annealing conditions, such as the gas ratio (H_2: NH_3, with a constant total flow rate), annealing temperature, and annealing time, have been explored previously.[12] Annealing times of 15, 30, 45, and 60 min were used for nitridation of four different samples. GaN was then overgrown at 1030 °C with constant TMGa and NH_3 flow rates of 156 μmol/min and 7 *l*/min, respectively, maintaining a V/III ratio of 2000. The overall thickness was ~7.5 μm. For comparison, a control GaN layer was grown on the same GaN template using identical growth conditions but without the TiN network.

To investigate the structural quality of the samples, both symmetric (0002) and asymmetric $(10\bar{1}2)$ x-ray diffraction peaks were measured using a Philips X'Pert MRD system equipped with a four-crystal Ge (220) monochromator. Continuous-wave (cw) PL was measured at temperatures as low as 10 K using a 25 mW HeCd laser operating at 325 nm (3.82 eV). Detection was performed by photon counting using a photomultiplier tube attached to a 1.25 m grating spectrometer. TRPL spectroscopy was employed at room temperature using a ~45 ps resolution Hamamatsu streak camera. Pulsed excitation was from a 1 kHz optical parametric amplifier with ~100 fs-wide pulses. The 3.82 eV excitation was incident 45° to the surface normal, and the TRPL was collected normal to the surface. The excitation density (~200 μJ/cm^2) was kept well below the stimulated emission threshold to measure the decay times.

TABLE I. XRD and 10 K PL linewidths, and TRPL decay constants and amplitude ratios (at 200 μJ/cm^2 excitation density) for GaN thin-layer samples grown with single (s-SiN) and double (d-SiN) SiN layers on low-temperature GaN buffer layers.

Sample	10 K PL D^0X (meV)	XRD (0002), $(10\bar{1}2)$ (arc min)	τ_1 τ_2 (ns)	A_2/A_1
Control	17.7	10.7, 26	0.04, 0.15	0.03
s-SiN	17.1	10.9, 15.6	0.09, 0.18	0.27
d-SiN	13.0	9.6, 12	0.10, 0.29	0.61

III. RESULTS AND DISCUSSION

Cross-sectional transmission electron microscope (TEM) analysis of a 1.5 μm-thick GaN sample with a single SiN nanonetwork layer deposited on a 100 nm-thick LT-GaN buffer showed a significant reduction in the TD density (mid-10^8 cm^{-2}) compared to the sample with no SiN network (mid-10^9 cm^{-2}).[8] With increasing GaN thickness and with the deposition of a second SiN layer, the TD density is expected to decrease further. It is found that the GaN growth starts from inside the pores in the SiN film, resulting in the formation of GaN islands during the initial stages of growth. These GaN islands subsequently grow laterally over the SiN covered area and, finally, a fully coalesced film is achieved. TEM images show that the porous SiN layer effectively blocks the vertical propagation of a majority of threading dislocations through the overgrown GaN, leading to an order of magnitude reduction in the dislocation density. In addition, the dislocations also bend during the growth of the islands and penetrate through the SiN layer, increasing their chances of combining and annihilating each other.

TEM measurements on TiN network samples indicate that thin and extended surface voids are formed above the discontinuous TiN layer, resulting in the lateral overgrowth of GaN.[12] The TDs in the GaN template are blocked by the TiN layer, and many of the TDs penetrating through the TiN windows to the upper layer change their propagation direc-

TABLE II. XRD and 10 K PL linewidths, and TRPL decay constants and amplitude ratios (at 200 μJ/cm^2 excitation density) for GaN thin-layer samples grown with single (s-SiN) and double (d-SiN) SiN layers on high-temperature GaN buffer layers. The PL FWHM values are obtained by fitting to the high-energy side of the D^0X peak, since there is too much broadening on the low-energy side.

Sample	10 K PL D^0X (meV)	XRD (0002), $(10\bar{1}2)$ (arc min)	τ_1, τ_2 (ns)	A_2/A_1
Control	3.9	4.7, 8.5	0.04, 0.54	0.04
s-SiN	4.2	3.6, 4.9	0.16, 0.45	0.30
d-SiN	3.6	4.3, 5.2	0.10, 0.85	0.62

TABLE III. XRD and 10 K PL linewidths, and TRPL decay constants and amplitude ratios (at 200 $\mu J/cm^2$ excitation density) for GaN thin-layer samples grown with single (s-SiN) and double (d-SiN) SiN layers on high-temperature AlN buffer layers.

Sample	10 K PL D^0X (meV)	XRD (0002), $(10\bar{1}2)$ (arc min)	τ_1,τ_2 (ns)	A_2/A_1
Control	4.3	8.2, 7.9	0.13, 0.32	0.06
s-SiN	2.3	7.8, 8.4	0.20, 0.45	0.42
d-SiN	2.3	7.5, 4.4	0.29, 0.77	0.38

tion and extend laterally. As a result, the density of threading dislocations significantly decreases at and above the TiN/GaN interface ($\sim 10^8$ cm^{-2}).

Supporting these observations are the x-ray diffraction (XRD) results in Tables I–IV. The full width at half maximum (FWHM) of the $(10\bar{1}2)$ peak is decreased for the samples with SiN and TiN networks, which generally suggests the reduction of edge and mixed TDs. The addition of the second SiN layer shows further improvement except for the HT-GaN buffer layer sample. It is also seen that the FWHM of the $(10\bar{1}2)$ peak decreased with further nitridation in TiN network samples. To ascertain whether the reduction of TDs actually reduces the nonradiative pathways, low-temperature PL and room-temperature TRPL measurements were performed on all the samples.

10-K PL spectra for double-layer SiN samples from each set are shown in Fig. 1. The inset shows an enlarged view of the band-edge spectral region. It is clear that the sample with the high-temperature AlN buffer layer exhibits stronger band-edge excitonic features, where the *A*-free exciton (FX_A) and donor-bound exciton (D^0X) transitions are easily distinguished at 3.488 and 3.483 eV, respectively. The intensity of the band-edge emission is increased for samples with SiN layers and is higher for the samples grown on AlN buffer layers. The yellow and blue emission bands are about an order of magnitude weaker than the band-edge emission. As listed in Tables I–III, the FWHM of the D^0X peak obtained from Gaussian fits decreases with the addition of the SiN layers. Samples with SiN layers on AlN buffer layers have a PL FHWM of 2.3 meV, indicating that high optical quality can be achieved with the inclusion of the SiN porous network.

TABLE IV. XRD and 10 K PL linewidths, and TRPL decay constants and amplitude ratios (at 200 $\mu J/cm^2$ excitation density) for GaN thin-layer samples grown on TiN templates. Data for the control sample with no TiN layer and a freestanding GaN sample are also included.

Sample	10 K PL FX_A, D_0X (meV)	XRD (0002), $(10\bar{1}2)$ (arc min)	τ_1, τ_2 (ns)	A_2/A_1
15 min	3.2, 3.9	6.4, 6.1	0.47, 1.86	0.59
30 min	3.8, 4.5	5.8, 4.9	0.39, 1.32	0.58
45 min	4.0, 5.3	5.1, 4.6	0.45, 1.68	0.54
60 min	3.4, 3.2	5.9, 4.6	0.41, 1.54	0.52
Control	3.1, 3.2	5.6, 7.1	0.13, 0.30	0.36
Freestanding GaN			0.34, 1.73	0.33

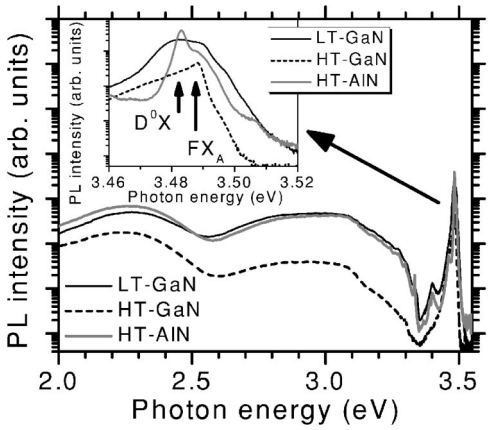

FIG. 1. 10 K PL spectra for the double-layer SiN network samples. The inset shows the free exciton region of the spectra.

Figure 2 shows the 10 K PL spectra for the GaN epilayer samples with TiN subjected to 15 and 60 min nitridation and the control sample with no TiN. All four samples (30 and 45 min nitridation samples not shown) exhibit strong excitonic features around the band edge. The blue and yellow luminescence bands are also visible but are as much as two orders of magnitude weaker than the band-edge emission in all the samples. An enlarged view of the band-edge spectral region is shown in the inset of Fig. 2, where the free exciton peaks at 3.491, 3.499, and 3.511 eV indicate the FX_A, the FX_B, and the FX_A excited-state transitions, respectively. The main donor-bound exciton (D^0X) emission is observed at 3.485 eV. The FWHM of the FX_A and the D^0X peaks are given in Table IV. Another donor-bound exciton peak at 3.471 eV, which is not observed for the control sample, is visible for the samples with TiN network. The intensity of this peak is an order of magnitude larger for the 15 min nitridation sample than for the other samples. We suspect that the number of Ti impurities in overgrown GaN is reduced with increasing nitridation and that the 3.471 eV PL line may be related to these impurities.

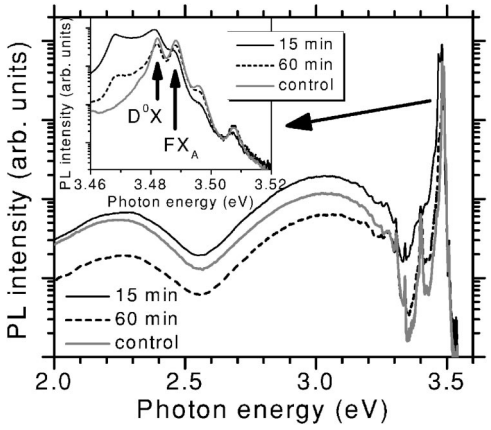

FIG. 2. 10 K PL spectra for the 15 and 60 min nitridation TiN network samples and the control sample. The inset shows the free exciton region of the spectra.

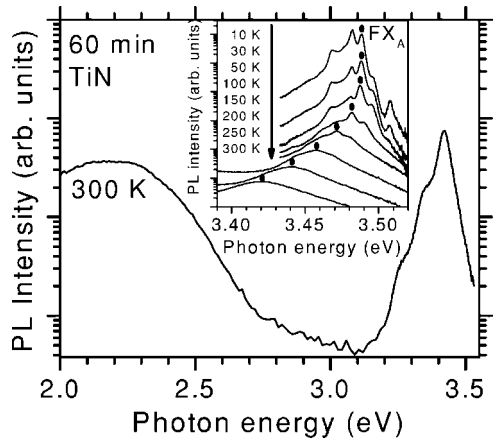

FIG. 3. Room-temperature PL spectrum for the 60 min nitridation TiN network sample. The inset shows the temperature dependence of the free exciton region. The peaks marked with filled circles show the evolution of the *A*-free exciton (FX_A) peak.

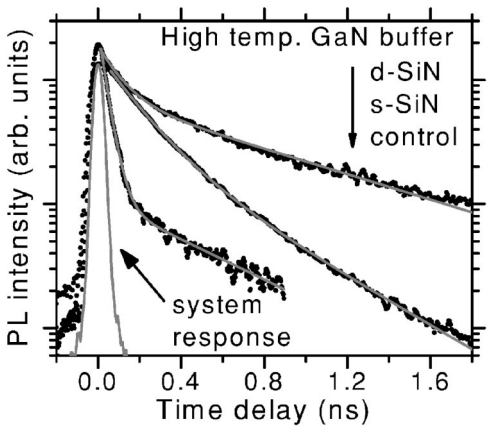

FIG. 5. Normalized time-resolved PL spectra for the SiN network samples with high-temperature GaN buffer layers. The solid lines are biexponential fits to the data.

To verify the excitonic peak assignments, temperature-dependent PL measurements were performed on the 60-min nitridation sample. In the 300 K PL of Fig. 3, the blue band dissappears, the band-edge emission redshifts to 3.422 eV, and the ratio of the band-edge luminescence to the yellow luminescence decreases. The inset of Fig. 3 shows the evolution of the FX_A peak with increasing temperature. Bound exciton peaks are visible up to 50 K, and only the FX_A and FX_B peaks remain above 100 K. The strong thermal quenching of the bound excitons comes from the increasing rate of excitation to the free exciton continuum.

The excitonic fine structure and the narrow linewidths at low temperatures are measures of the quality of the samples; however, it is not possible to come to a conclusion about the radiative efficiency from cw PL. TRPL is a nondestructive and powerful technique commonly used for the characterization of excess carrier dynamics in semiconductors. Since most optical and electrical devices are operated at room temperature, understanding the fundamental excess carrier recombination dynamics at 300 K is required to evaluate the relevant radiative and nonradiative recombination mechanisms and thus to improve the performance of devices. The efficiency of the radiative recombination, and therefore the material quality, is strongly related to the decay time of the particular transition. There is a limited number of reports related to the TRPL lifetimes of excess carriers in GaN at 300 K. Kwon *et al.*[13] reported a biexponential decay with 150 and 740 ps time constants for high-quality Si-doped MOCVD-grown GaN/sapphire. Decay times between 205 and 530 ps were measured for thick HVPE-grown templates,[14–16] and values ranging from 445 (Ref. 17) to 506 ps (Ref. 16) were reported for homoepitaxially grown GaN layers. In addition, Chichibu *et al.*[18] and Izumi *et al.*[19] reported biexponential decays with lifetimes τ_1 and τ_2 of 130 and 400 ps, and 80 and 459 ps, respectively, for GaN/sapphire films grown using ELO. However, the same groups obtained longer biexponential lifetimes of 130 and 860 ps (Ref. 18), and 98 and 722 ps (Ref. 19) for bulk GaN.

Figures 4–6 show the TRPL data for the SiN network samples with LT-GaN, HT-GaN, and HT-AlN buffer layers, respectively. The decays for all the samples were well characterized by a biexponential decay function $A_1 \exp(-t/\tau_1) + A_2 \exp(-t/\tau_2)$. Tables I–III summarize the decay constants and the amplitude ratios (A_2/A_1) obtained from the fits using the Levenberg–Marquardt algorithm.[20] Biexponential decays

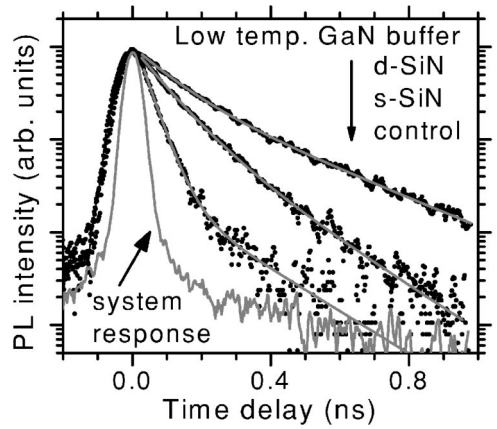

FIG. 4. Normalized time-resolved PL spectra for the SiN network samples with low-temperature GaN buffer layers. The solid lines are biexponential fits to the data.

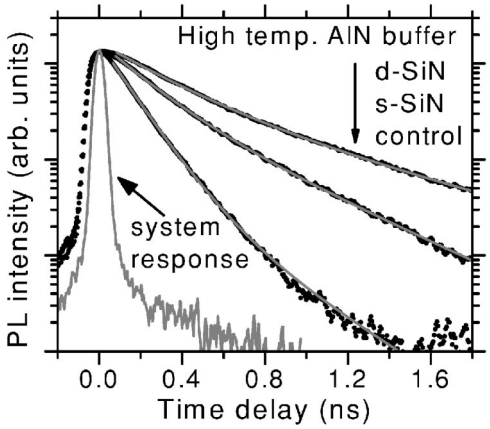

FIG. 6. Normalized time-resolved PL spectra for the SiN network samples with high-temperature AlN buffer layers. The solid lines are biexponential fits to the data.

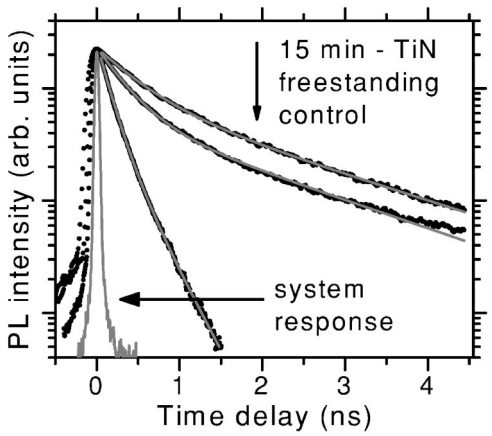

FIG. 7. Normalized time-resolved PL spectra for the 15 min nitridation TiN network sample, control sample, and freestanding GaN. The solid lines are biexponential fits to the data.

are characteristic of capture and recombination processes in a multilevel system. They may here be interpreted as related to the capture into deeper (nonradiative) centers, either in the bulk or at the surface/interface of the layer, followed by recombination. Although the biexponential decay times τ_1 and τ_2 most probably do not represent the pure nonradiative and radiative lifetimes, respectively, the ratio A_2/A_1 is suggestive of the relative importance of radiative decay. Thus, the particularly large ($A_2/A_1 > 0.5$) magnitude for the slow decaying components suggests increased radiative efficiency. Since the defect and the dislocation density may not be uniform, the photoexcited area may contain two regions having different recombination times. Therefore, the measured lifetimes τ_1 and τ_2 are both limited by nonradiative recombination, so longer decay lifetimes and larger A_2/A_1 ratios indicate reduced nonradiative relaxation.

For all three sets of samples, the decay times and the A_2/A_1 ratio generally increase with the addition of each SiN layer. For the set with the HT-GaN buffer, the control sample has a longer τ_2 but much smaller A_2/A_1 ratio than the single SiN layer sample, and the double SiN layer sample has a shorter τ_1, but almost two times longer τ_2 than the single SiN layer sample. With the addition of the second SiN layer the A_2/A_1 ratio stays nearly the same for the HT-AlN samples; however, the decay times increase significantly.

Figure 7 shows the TRPL data for the TiN network samples (15 min nitridation sample and the control sample) and a HVPE-grown 200 μm-thick freestanding GaN. The decay constants and the amplitude ratios obtained from biexponential fits for 200 $\mu J/cm^2$ excitation (an estimated photogenerated carrier density of $\sim 10^{17}$ cm^{-3}) are listed in Table IV. The decay times for the samples with TiN network layers are significantly larger than those for the samples with SiN network layers. The 15 min nitridation sample exhibits decay times of $(\tau_1, \tau_2) = (0.47\ \text{ns}, 1.86\ \text{ns})$. With decreasing excitation energy density, the decay times slightly decreased [e.g., $(\tau_1, \tau_2) = (0.34\ \text{ns}, 1.60\ \text{ns})$ for 20 $\mu J/cm^2$ excitation of the 15 min nitridation sample] for all the samples. The longer carrier lifetimes observed at higher photogenerated carrier densities may be attributed to the saturation of trap states.[16] This will result in more carriers recombining through relatively slower band-to-band radiative recombination. Moreover, since both decay constants increase but A_2/A_1 remains constant (e.g., $A_2/A_1 = 0.55$ for 20 $\mu J/cm^2$ excitation for the 15 min nitridation sample) with increasing excitation, we can also rule out the partial contribution from bimolecular recombination,[19] which has an estimated characteristic decay time of around 1.6 ns for a 10^{19} cm^{-3} carrier density.[12]

IV. CONCLUSIONS

The improvement in decay times for the samples with SiN and TiN templates compared to the control GaN samples reflects the fact that TDs act as nonradiative recombination channels. However, no direct correlation is observed between the XRD linewidths and the decay times within the SiN and TiN network samples. For samples with a low density of TDs, it has been suggested that the very short diffusion length of carriers in GaN prevents most of the carriers from being trapped into TDs.[18] Therefore, the observed sample-to-sample variation in the decay times may be ascribed to point-defect-like nonradiative centers that cannot be detected by the TEM. Similar TRPL decay times measured from the wing and the window regions of ELO-GaN samples, wing region having almost four orders of magnitude smaller TD density ($<10^6$ cm^{-2}), support this argument.[18,19] These results indicate that threading dislocations do not limit the emission efficiency at room temperature as much as other types of nonradiative recombination centers like point defects and impurities.

In short, growth of GaN thin films on SiN and TiN porous network templates significantly improves the structural quality and the radiative efficiency of the overgrown layer. In terms of the decay times, the samples with TiN network show much better performance (almost two times increase in decay times) than the samples with SiN network. The slow decaying component for the 15 min nitridation sample has a $\tau_2 = 1.86$ ns time constant that is comparable with the result of $\tau_2 = 1.73$ ns from a 200 μm-thick freestanding GaN, but has a relative magnitude (A_2/A_1) almost twice as large.

ACKNOWLEDGMENTS

This work was supported by a DURINT program administered by ONR (Dr. C. E. C. Wood). The research also benefited from grants from AFOSR (Dr. T. Steiner and Dr. G. L. Witt). The Duke portion of this work was funded in part by U.S. Army Research Office Grant No. W011NF-04-D-0001/DI #0002. The authors would like to thank Professor R. M. Feenstra of Carnegie Mellon University, Professor T. S. Kuan of SUNY Albany, and Professor D. J. Smith of Arizona State University for their critical contributions to the development of SiN- and TiN-nanonetwork-based GaN by MOCVD.

[1] H. Morkoç, *Nitride Semiconductors and Devices* (Springer, Berlin, 1999).
[2] M. A. Reshchikov and H. Morkoç, J. Appl. Phys. (in press).
[3] P. Visconti, K. M. Jones, M. A. Reshchikov, F. Yun, R. Cingolani, H. Morkoç, S. S. Park, and K. Y. Lee, Appl. Phys. Lett. **77**, 3743 (2000).
[4] Y. Oshima, T. Eri, M. Shibata, H. Sunakawa, and A. Usui, Phys. Status Solidi A **194**, 554 (2002).
[5] P. Gibart, B. Beaumont, and P. Vennéguès, in *Handbook on Materials and Devices*, edited by P. Ruterana, M. Albrecht, and J. Neugebauer (Wiley-

VCH, Weinheim, 2003).
[6]S. Haffouz, B. Beaumont, P. Vennegues, and P. Gibart, Phys. Status Solidi A **176**, 677 (1999).
[7]S. Sakai, T. Wang, Y. Morishima, and Y. Naoi, J. Cryst. Growth **221**, 334 (2000).
[8]A. Sagar, R. M. Feenstra, C. K. Inoki, T. S. Kuan, Yi Fu, Y. T. Moon, and H. Morkoç, International Workshop on Nitride Semiconductors, Pittsburgh, PA, 2004 (unpublished); Phys. Status Solidi A **202**, 722 (2005).
[9]X. L. Fang, Y. Q. Wang, H. Meidia, and S. Mahajan, Appl. Phys. Lett. **84**, 484 (2004).
[10]Y. Oshima, T. Eri, M. Shibata, H. Sunakawa, and A. Usui, Phys. Status Solidi A **194**, 554 (2002).
[11]P. Visconti, K. M. Jones, M. A. Reshchikov, F. Yun, R. Cingolani, H. Morkoç, S. S. Park, and K. Y. Lee, Appl. Phys. Lett. **77**, 3743 (2000).
[12]Y. Fu *et al.*, Appl. Phys. Lett. **86**, 043108 (2005).
[13]H. K. Kwon, C. J. Eiting, D. J. H. Lambert, M. M. Wong, R. D. Dupuis, Z. Liliental-Weber, and M. Benamara, Appl. Phys. Lett. **77**, 2503 (2000).
[14]G. E. Bunea, W. D. Herzog, M. S. Ünlü, B. B. Goldberg, and R. J. Molnar, Appl. Phys. Lett. **75**, 838 (1999).
[15]S. Juršėnas, S. Miasojedovas, G. Kurilčik, A. Žukauskas, and P. R. Hageman, Phys. Status Solidi A **201**, 199 (2004).
[16]A. V. Sampath *et al.*, J. Vac. Sci. Technol. B **22**, 1487 (2004).
[17]S. Juršėnas *et al.*, Appl. Phys. Lett. **78**, 3776 (2001).
[18]S. F. Chichibu *et al.*, Appl. Phys. Lett. **74**, 1460 (1999).
[19]T. Izumi, Y. Narukawa, K. Okamoto, Y. Kawakami, Sg. Fujita, and S. Nakamura, J. Lumin. **87–89**, 1196 (2000).
[20]W. H. Press, B. P. Flannery, S. A. Tuekolsky, and W. T. Vetterling, *Numerical Recipes in C: The Art of Scientific Computing* (Cambridge University Press, Cambridge, 1988).